The horizontal intrusion layer of melt in a saturated porous medium

A. Bejan and Z. Zhang
Department of Mechanical Engineering and Materials Science, Duke University, Durham, NC, USA

P. Jany
Department of Mechanical Engineering, Fachhochshule Ravensburg-Weingarten, Weingarten, Federal Republic of Germany

This article presents a theory of how the melt region advances as an intrusion layer along the top boundary of a solid phase-change material that is heated from the side. The phase-change material fills the pores of a solid matrix. We show that the thickness of the horizontal melt layer increases as $x^{3/5}$, where x is the horizontal distance measured away from the leading edge of the layer. The total length of the intrusion layer increases as $t^{3/4}$, and as $T_{max}^{5/4}$. Finite-difference simulations of convection melting in the Darcy–Rayleigh number range of 200–800 agree with the theoretical results. We also show that in a rectangular porous medium heated from the side, the size of the entire melt region is dominated by the melting contributed by the horizontal intrusion layer, if the time is great enough so that the group $(\mathrm{Ste\,Fo})^{1/4}$ is greater than 1.

Keywords: porous medium; melting; natural convection

Introduction

The convection melting phenomenon described in this article is related to the melting of a block of phase-change material that is suddenly subjected to heating from the side. The voluminous work that has already been devoted to this problem showed that natural convection plays a significant role, especially in the late stages of the melting process.

The most visible aspect of the natural convection effect is the deformed and constantly changing shape of the two-phase interface. The interface is straight and vertical only in the very beginning of the process, when the dominant heat transfer mechanism is conduction. In the convection dominated regime (known also as the quasi-steady regime), the interface acquires a characteristic shape the dominant feature of which is a horizontal layer of melt that grows along the top boundary of the phase-change system. The slenderness of the horizontal layer increases with time and the Rayleigh number. This behavior has been documented most recently by Lacroix[1] in phase-change materials melting near a vertical isothermal wall and by Zhang and Bejan[2] near a wall heated at constant rate. It has also been observed in a porous medium saturated with a phase-change material.[3]

With these images in mind, the deformed liquid region can be viewed as the union of two simpler regions: an upper zone that is a horizontal intrusion layer and a lower zone that houses a vertical counterflow. These two zones are labeled A_2 and A_1 in Figure 1.

The complicated and unsteady shape of the melting front is the main reason why it has been difficult to treat analytically the convection dominated regime of the melting process when the heating is from the side. The theoretical descriptions that have been attempted for melting due to heating from the side are all based on the approximation that the two-phase interface is sufficiently vertical over its entire height.[3–6] Kazmierczak *et al.*[4] also solved the problem of melting on a horizontal surface.

In this article we focus on the properties of the horizontal layer of melt that propagates into the solid region, along the top boundary of the system. We are particularly interested in the shape and propagation speed of this melt subregion. Our ultimate objective is to determine when and to what extent this horizontal intrusion layer dominates the size and growth rate of the entire region that is filled with liquid.

We consider the case of a phase-change material that fills the pores of a solid matrix. We decided to study the problem of convection melting in a saturated porous medium instead of the more common problem of convection melting in a pure phase-change material (without porous matrix), because we had access to a set of numerical simulations of the porous-medium version of the problem;[3] against these numerical results we tested the theoretical solution that emerged.

Physical model

Consider the horizontal melt layer shown separately in Figure 2 and assume that it is slender enough that its local depth $\delta(x)$ is considerably smaller than the distance to the leading edge of the layer, or

$$\delta(x) \ll x \tag{1}$$

As long as this assumption holds, the steady-state conservation equations for mass, momentum, and energy in the x–y frame are of the boundary-layer type (see, for example, Cheng[7]):

$$\frac{\partial^2 \psi}{\partial y^2} = -\frac{Kg\beta}{\nu}\frac{\partial T}{\partial x} \tag{2}$$

$$\frac{\partial \psi}{\partial y}\frac{\partial T}{\partial x} - \frac{\partial \psi}{\partial x}\frac{\partial T}{\partial y} = \alpha \frac{\partial^2 T}{\partial y^2} \tag{3}$$

Address reprint requests to Professor Bejan at the Department of Mechanical Engineering and Materials Science, Duke University, Durham, NC 27706, USA.

Received 3 October 1989; accepted 26 February 1990

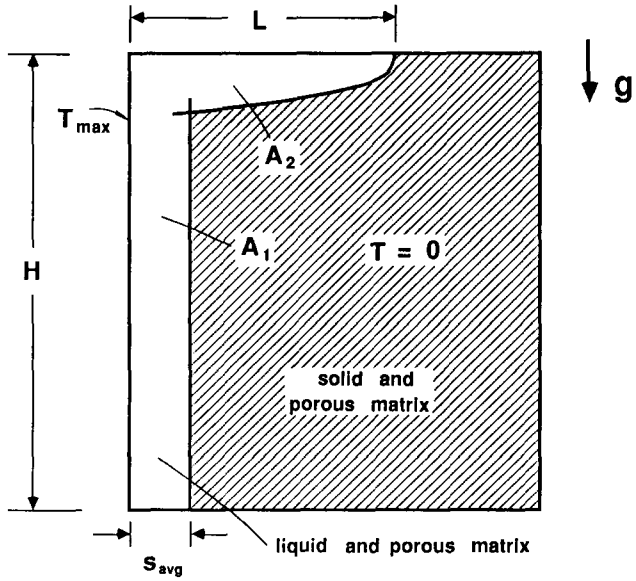

Figure 1 Two-zone model (A_1+A_2) for the melt region of a rectangular system heated from the side

Equations 2 and 3 are based on the homogeneous porous-medium model, in which α is the ratio of the thermal conductivity of the liquid-saturated porous matrix divided by the heat capacity (ρc) of the liquid alone. The temperature T is the local equilibrium temperature of both the liquid and the matrix. The momentum Equation 2 is based on the Darcy flow model in which K is the permeability constant of the porous medium. The liquid is being modeled as Newtonian and Boussinesq incompressible, with constant kinematic viscosity ν and constant coefficient of thermal expansion β. The stream function ψ is defined in such a way that $\partial\psi/\partial y$ is the horizontal liquid velocity (in the positive x direction), and $-\partial\psi/\partial x$ is the vertical liquid velocity (in the positive y direction). These liquid-velocity components are volume-averaged quantities.

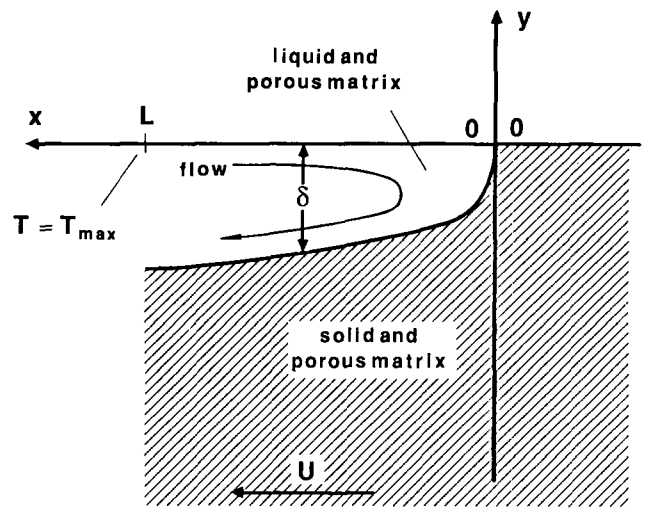

Figure 2 Horizontal melt layer intruding into an isothermal porous medium saturated with phase-change material at the melting point (region A_2 of Figure 1)

The origin of the x–y frame is attached to the leading edge of the liquid region. Let U be the actual melting speed, that is, the velocity with which the leading edge travels into the region saturated with solid phase-change material. Relative to the x–y frame then, the solid (the region under the melt layer) moves to the left with velocity U. We show later (in Equation 30) that it is reasonable to assume that the melting speed U is small compared to the order of magnitude of the horizontal velocity of the liquid; that is,

$$U \ll O\left(\frac{\partial\psi}{\partial y}\right) \tag{4}$$

Another assumption recommended by visual observations of the melting-front shape is that the shape of the horizontal liquid layer is preserved in the x–y frame. This assumption means that the liquid depth δ is a function of x only. (The

Notation

A_1	Area of melt region due to vertical boundary-layer convection, Figure 1
A_2	Area of melt region due to the horizontal intrusion layer, Figure 1
c	Specific heat of liquid
C	Constant, Equation 37
F	Similarity stream-function profile, Equation 17
Fo	Fourier number, $\mathrm{Fo}=\alpha t/H^2$
g	Gravitational acceleration
h_{sf}	Latent heat of melting
H	Height
k	Thermal conductivity of saturated porous medium
K	Permeability
l	Horizontal dimension of rectangular enclosure, Figure 6
L	Length of intrusion layer, Figure 6
Ra	Rayleigh number based on ΔT, Equation 13
$\mathrm{Ra_H}$	Rayleigh number based on T_{max}, Equation 38
s_{avg}	Average thickness of vertical-gap portion of the melt region, Figure 1
Ste	Liquid-saturated porous medium Stefan number, $\mathrm{Ste}=cT_{max}/\phi h_{sf}$
t	Time
T	Excess temperature above the melting point
T_{max}	Overall (maximum) temperature difference across the melt region
ΔT	Temperature factor (constant)
U	Speed of propagation of the horizontal intrusion layer
V	Vertical "blowing" velocity due to melting, Equation 26
x	Horizontal coordinate, Figure 2
y	Vertical coordinate, Figure 2

Greek symbols

α	Thermal diffusivity of saturated porous medium, $\alpha=k/(\rho c)$
β	Volumetric coefficient of thermal expansion
δ	Thickness of horizontal intrusion layer
η	Similarity variable, Equation 19
θ	Similarity temperature profile, Equation 18
ν	Kinematic viscosity
ρ	Density of phase-change material (liquid or solid)
ϕ	Porosity
ψ	Stream function

Table 1 Summary of the simplifying assumptions on which the intrusion-layer analysis is based

- Slender horizontal melt layer
- Isothermal solid at the melting point (no conduction in the solid)
- Homogeneous porous medium model
- Darcy flow
- Newtonian and Boussinesq incompressible liquid, with constant ν and β
- Liquid density equal to density of solid
- Melting speed U small relative to horizontal liquid velocity (or small Stefan number)
- Melting-front shape preserved in time (in the x–y frame of Figure 1)

same assumption is implicit in the writing of the steady-state Equations 2 and 3.)

The melting that occurs at the bottom of the liquid layer is the result of the balance between the local vertical heat flux that lands on the two-phase interface and the rate of the latent heat release at the interface:

$$k\left(\frac{\partial T}{\partial y}\right)_{y=-\delta}=\rho\phi h_{sf}\frac{d\delta}{dx}U \tag{5}$$

where ϕ is the porosity of the matrix.[3] The simplicity of the interface condition, Equation 5, is due to two simplifying assumptions of the present model. First, there is no conduction into the solid region, because the solid is assumed to be isothermal and at the melting point (i.e., there is no solid subcooling, $T=0$). Second, the liquid density ρ is assumed to be equal to the density of the solid. The assumptions on which the present model is based are summarized in Table 1.

Similarity formulation

The flow and temperature distributions in the liquid-saturated region can be described by means of a similarity solution. The analytical form of this solution becomes evident if we examine the scaling implications of Equations 2, 3, and 5, namely,

$$\frac{\psi}{\delta^2}\sim\frac{Kg\beta}{\nu}\frac{T}{x} \tag{6}$$

$$\frac{\psi}{x\delta}\sim\frac{\alpha}{\delta^2} \tag{7}$$

$$k\frac{T}{\delta}\sim\rho\phi h_{sf}\frac{\delta}{x}U \tag{8}$$

Solving this system for δ, ψ, and T, we find that

$$\delta\sim x^{3/5}\left(\frac{\alpha\nu}{Kg\beta}\frac{k}{\rho\phi h_{sf}U}\right)^{1/5} \tag{9}$$

$$\psi\sim x^{2/5}\alpha\left(\frac{Kg\beta}{\alpha\nu}\frac{\rho\phi h_{sf}U}{k}\right)^{1/5} \tag{10}$$

$$T\sim x^{1/5}\left(\frac{\alpha\nu}{Kg\beta}\right)^{2/5}\left(\frac{\rho\phi h_{sf}U}{k}\right)^{3/5} \tag{11}$$

Of particular interest is the x dependence of these quantities. Note that the melt-layer depth increases as $x^{3/5}$ away from the leading edge. The temperature of the melt region increases as $x^{1/5}$ away from the leading edge, where the temperature is equal to the melting point temperature ($T=0$). At the other end (the deep end) of the melt region, $x=L$, the scale of the temperature T is dictated by the overall temperature difference that drives the melting process. Let ΔT be an approximate estimate of the overall temperature difference. Substituting $x=L$ and $T\sim\Delta T$ into Equation 1, we obtain

$$U\frac{\rho\phi h_{sf}L}{k\,\Delta T}\sim\widetilde{\mathrm{Ra}}^{2/3} \tag{12}$$

where $\widetilde{\mathrm{Ra}}$ is a "temporary" Darcy-modified Rayleigh number based on the horizontal dimension of the liquid region L and on the unknown (constant) temperature difference scale ΔT:

$$\widetilde{\mathrm{Ra}}=\frac{Kg\beta L\Delta T}{\alpha\nu} \tag{13}$$

The relationship between the temporary constant ΔT and the actual (maximum) temperature difference that drives the melting process ($T_{\max}$) is one of the objectives of this analysis (see Equation 32).

We can now use the melting speed scale, Equation 12, to rewrite Equations 9–11 in dimensionless form:

$$\frac{\delta}{L}\sim\left(\frac{x}{L}\right)^{3/5}\widetilde{\mathrm{Ra}}^{-1/3} \tag{14}$$

$$\frac{\psi}{\alpha}\sim\left(\frac{x}{L}\right)^{2/5}\widetilde{\mathrm{Ra}}^{1/3} \tag{15}$$

$$\frac{T}{\Delta T}\sim\left(\frac{x}{L}\right)^{1/5} \tag{16}$$

These relations provide the basis for a similarity solution of the form:

$$\psi=\alpha\widetilde{\mathrm{Ra}}^{1/3}\left(\frac{x}{L}\right)^{2/5}F(\eta) \tag{17}$$

$$T=\Delta T\left(\frac{x}{L}\right)^{1/5}\theta(\eta) \tag{18}$$

in which the similarity variable η is defined as the ratio y/δ; that is,

$$\eta=\widetilde{\mathrm{Ra}}^{1/3}\frac{y}{L}\left(\frac{x}{L}\right)^{-3/5} \tag{19}$$

The lower boundary of the melt layer (the melting front) is represented by $\eta=-1$; the upper surface of the melt layer is located at $\eta=0$.

Substitution of Equations 17–19 into momentum and energy Equations 2 and 3 leads to a system for the similarity stream-function and temperature profiles, $F(\eta)$ and $\theta(\eta)$:

$$-\tfrac{1}{5}\theta+\tfrac{3}{5}\eta\theta'=F'' \tag{20}$$

$$\tfrac{1}{5}\theta F'-\tfrac{2}{5}F\theta'=\theta'' \tag{21}$$

in which $(\ )'=d(\ )/d\eta$ and $(\ )''=d^2(\ )/d\eta^2$. Equations 20 and 21 must be subjected to the conditions that the upper boundary is impermeable and adiabatic,

$$F(0)=0,\qquad \theta'(0)=0 \tag{22, 23}$$

and that the lower boundary (the melting front) is impermeable and isothermal,

$$F(-1)=0,\qquad \theta(-1)=0 \tag{24, 25}$$

The impermeable melting-front condition, Equation 24, is an approximation that is valid as soon as the slow-melting assumption, Equation 4, holds. This result can be demonstrated by noting that (cf., mass conservation) the scale of the vertical "blowing" velocity V due to melting at the $y=-\delta(x)$ interface is related to the translational melting speed U:

$$VL\sim U\delta \tag{26}$$

The impermeable melting-front approximation, Equation 24,

is valid when V is small relative to the vertical velocity scale in the liquid-saturated region:

$$V \ll O\left(-\frac{\partial \psi}{\partial x}\right) \tag{27}$$

that is, when

$$V \ll \frac{\psi}{L} \tag{28}$$

In view of Equations 14, 15, and 26, and recognizing that $x \sim L$, we see that the inequality 28 becomes

$$U \ll \frac{\alpha}{L} \widetilde{\mathrm{Ra}}^{2/3} \tag{29}$$

It is not difficult to show that the same small-U inequality is obtained by starting with the assumption of Equation 4 and using the results, Equations 14 and 15. Finally, by combining Equations 12 and 29, we reach the conclusion that the impermeable interface assumption is valid when the Stefan number is small, or

$$\frac{c\,\Delta T}{\phi h_{sf}} \ll 1 \tag{30}$$

Results

The problem stated in Equations 20–25 was solved numerically by integrating from $\eta = -1$ to $\eta = 0$ in steps of size $\Delta\eta = 0.001$. The integration was based on the fourth-order Runge–Kutta method, the error being on the order of $(\Delta\eta)^5$. Starting guesses were made for the initial slopes of the stream-function and temperature profiles $F'(-1)$ and $\theta'(-1)$. The success of aiming for the end conditions, Equations 22 and 23, was judged in terms of how close the aggregate quantity $\{[F(0)]^2 + [\theta'(0)]^2\}$ approached zero.

Double precision was employed in all the calculations. Table 2 shows that the final similarity solution is practically insensitive to the size of the step $\Delta\eta$. Other features of this solution are

$$\begin{aligned} \theta'(-1) &= \ \ 108.484 \\ F'(0) &= -11.6858 \\ F'(-1) &= \ \ 21.3522 \end{aligned} \tag{31}$$

The stream-function profile $F(\eta)$ and the horizontal velocity profile $F'(\eta)$ are shown in Figures 3 and 4. The stream-function maximum F_{max} (i.e., the flow reversal) occurs at $\eta = -0.586$.

The similarity temperature profile is presented in Figure 5. In view of Equation 18 and the $\theta(0)$ value reported in the bottom line of Table 2, the overall (maximum) temperature difference that drives the horizontal melt layer is

$$T_{max} = T(x = L, \eta = 0) = \theta(0)\,\Delta T \tag{32}$$

This solution permits calculation of the slow speed of advancement of the melt layer U and the horizontal travel L as functions of time. Combining the interface condition, Equation 5, with Equation 18, and noting that $\delta = L(x/L)^{3/5}\widetilde{\mathrm{Ra}}^{-1/3}$, we

Table 2 The effect of integration step size on the overall characteristics of the similarity solution

$\Delta\eta$	F_{max}	$\theta(0)$
0.01	4.01596	63.2696
0.005	4.01591	63.2694
0.001	4.01544	63.2694

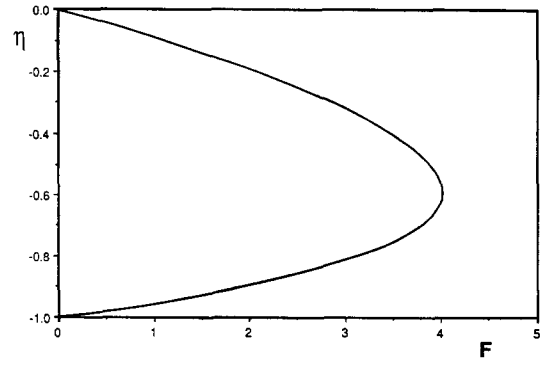

Figure 3 Similarity stream-function profile

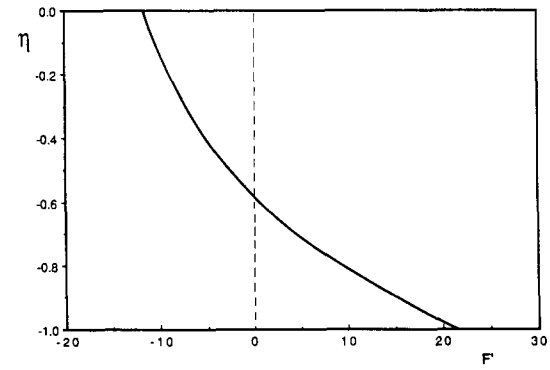

Figure 4 Similarity profile for horizontal velocity

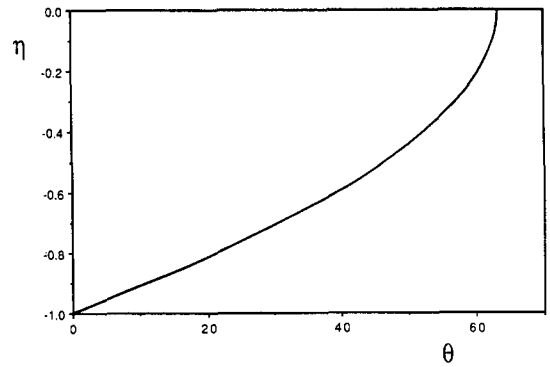

Figure 5 Similarity temperature profile across the melt layer

obtain

$$U\,\frac{\rho\phi h_{sf} L}{k\,\Delta T} = \tfrac{5}{3}\theta'(-1)\widetilde{\mathrm{Ra}}^{2/3} \tag{33}$$

With the kinematic relation between U and L,

$$U = \frac{dL}{dt} \tag{34}$$

Equation 33 becomes a first-order ordinary differential equation for the penetration length $L(t)$. Integrated from the initial condition $L(0) = 0$, this equation yields

$$L^{4/3} = \tfrac{20}{9}\theta'(-1)\left(\frac{Kg\beta\,\Delta T}{\alpha\nu}\right)^{2/3} \frac{k\,\Delta T}{\rho\phi h_{sf}}\, t \tag{35}$$

In this result, the temporary ΔT constant can be dropped in favor of the actual end-to-end temperature difference T_{max} (cf.,

Equation 32):

$$L=C\left(\frac{Kg\beta}{\alpha\nu}\right)^{1/2}T_{\max}^{5/4}\left(\frac{kt}{\rho\phi h_{sf}}\right)^{3/4} \tag{36}$$

in which the leading numerical coefficient C can be calculated with the help of Table 2 and the first of Equations 31:

$$C=[\tfrac{20}{9}\theta'(-1)]^{3/4}[\theta(0)]^{-5/4}=0.343 \tag{37}$$

The theoretical prediction provided by Equation 36 can be tested against numerical experiments[3] of natural convection melting in a rectangular domain of height H and overall length l. A sample of these numerical results is presented in Figure 6. The solid portion of the saturated porous medium is at the melting point temperature ($T=0$). The left side of the enclosure is heated suddenly to constant temperature $T_{\max}$ at time $t=0$. The penetration length of the horizontal melt region $L(t)$ can be measured along the upper boundary of the rectangular frame of the enclosure.

The numerical scheme on which Figure 6 is based was described in the earlier work[3] that dealt with the scale analysis and correlation of the calculated heat transfer rates. These numerical experiments were presented in terms of the Darcy-modified Rayleigh number based on the height H:

$$\mathrm{Ra}_H=\frac{Kg\beta HT_{\max}}{\alpha\nu} \tag{38}$$

and the dimensionless time group

$$\mathrm{Ste\,Fo}=\frac{kT_{\max}}{\rho\phi h_{sf}H^2}t \tag{39}$$

where Ste is the Stefan number based on $T_{\max}$, namely, $\mathrm{Ste}=cT_{\max}/\phi h_{sf}$. In terms of these old dimensionless groups, the theoretical melt-layer length, from Equations 36 and 37 reads

$$\frac{L}{H}=0.343\mathrm{Ra}_H^{1/2}(\mathrm{Ste\,Fo})^{3/4} \tag{40}$$

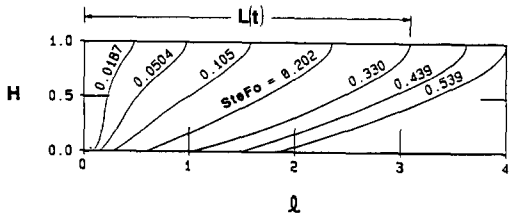

Figure 6 Numerical simulations[3] of the evolution of the melting front in a rectangular system heated from the side ($\mathrm{Ra_H}=800$, $l/H=4$)

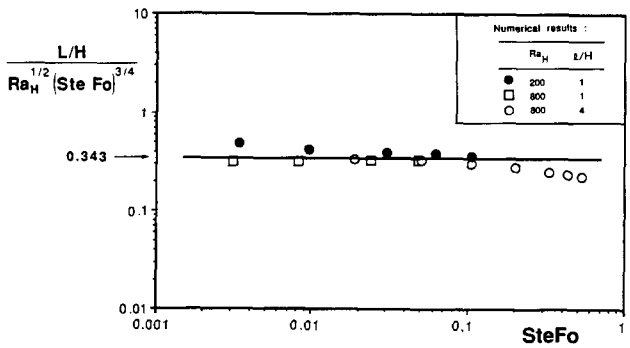

Figure 7 Total length of penetration of the horizontal layer: theory versus numerical experiments

Figure 7 shows a comparison between the numerical $(L/H)\mathrm{Ra_H}^{-1/2}(\mathrm{Ste\,Fo})^{-3/4}$ values deduced from Reference 3 and the theoretical constant 0.343. The numerical experiments were conducted in the $\mathrm{Ra_H}$ range of 200–800 and the l/H range of 1–4. Agreement between the numerical experiments and the present theory is very good. Noteworthy not only is the agreement between the theoretical and numerical trends (e.g., the fact that L increases as $\mathrm{Ra_H^{1/2}}$ and as $t^{3/4}$), but also the quantitative agreement between the theoretical coefficient 0.343 and the empirical (average) value revealed by numerical simulations of the phenomenon.

The numerical data begin to deviate from the theoretical line when the time Ste Fo increases beyond the point where the bottom boundary of the enclosure becomes bare (see Figure 6). Beyond this point, the total length of the melting front (the "driving" surface of the intrusion layer) is shorter than it would have been in the corresponding theoretical model of Figure 2. Consequently, the numerical value of the penetration length L should be smaller than the value predicted by the theory; this expectation is confirmed by the position of the rightmost numerical data relative to the theoretical line.

Conclusions

We have described theoretically the growth of the horizontal melt layer along the top boundary of a porous medium saturated with solid phase-change material. Applied to the problem of melting a rectangular system by heating it from the side, the present theory accounts for the most severe aspect of the deformation acquired by the melting front during the late stages of the melting process. Figure 7 proves that the present model works well and provides a useful alternative to full-scale numerical simulations. This alternative is much easier to use and provides the user with an acceptable degree of engineering accuracy.

As an application of the present results, consider the task of calculating the melt fraction (the space occupied by porous medium saturated with liquid) at sufficiently long times, when the melting process is dominated by convection. The simplest approach is to disregard the upper intrusion layer and to model the liquid-saturated region as a vertical layer in the natural convection boundary-layer regime (regime III in Reference 3). In the absence of significant liquid superheating, Equation 30, the relationship between melt fraction and time is determined easily, based on any of the theories of boundary-layer convection in vertical porous layers heated from the side. According to Weber,[8] for example, the average heat flux that arrives at the "nearly vertical" melting front is

$$q''_{\mathrm{avg}}=0.577\frac{kT_{\max}}{H}\mathrm{Ra_H^{1/2}} \tag{41}$$

Setting this heat flux equal to $\rho\phi h_{sf}\,ds_{\mathrm{avg}}/dt$, where s_{avg} is the average thickness of the vertical melt layer (profile area A_1 in Figure 1, where $A_1=s_{\mathrm{avg}}H$), we obtain

$$s_{\mathrm{avg}}=0.577\frac{kT_{\max}}{H}\mathrm{Ra_H^{1/2}}\frac{t}{\rho\phi h_{sf}} \tag{42}$$

This last step was based on the additional assumption that the time interval t is long enough that the development of s_{avg} is due primarily to the boundary-layer convection regime and not to the conduction dominated regime that sets in immediately after $t=0$. Noting again that $A_1=s_{\mathrm{avg}}H$, we can write the dimensionless counterpart of Equation 42 as

$$\frac{A_1}{H^2}=0.577\mathrm{Ra_H^{1/2}}(\mathrm{Ste\,Fo}) \tag{43}$$

We are now in a position to improve this classical result, by considering the two-area melt-region model shown in Figure 1. The present model has two distinct zones: the vertical gap A_1, treated in the preceding paragraph, and the horizontal intrusion layer of area A_2, length $L(t)$, and thickness $\delta(x)$. The profile area of the horizontal intrusion layer (see Figure 2) is

$$A_2 = \int_0^L \delta(x)\,dx = \tfrac{5}{8} L^2 \widetilde{\mathrm{Ra}}^{-1/3} \tag{44}$$

Using the main result of the intrusion-layer theory, Equation 40 and the relationship between $\widetilde{\mathrm{Ra}}$ and Ra_H (namely, Equations 13, 32, and 40), we can also write the area A_2 as

$$\frac{A_2}{H^2} = 0.419 \mathrm{Ra}_H^{1/2} (\mathrm{Ste\,Fo})^{5/4} \tag{45}$$

In conclusion, according to the two-area melt-region model of Figure 1, the dimensionless *total* area occupied by liquid-saturated porous medium is

$$\frac{A_1 + A_2}{H^2} = 0.577 \mathrm{Ra}_H^{1/2} (\mathrm{Ste\,Fo})[1 + 0.725(\mathrm{Ste\,Fo})^{1/4}] \tag{46}$$

The relative effect of the horizontal intrusion layer on the size of the melt region is described by the group $(\mathrm{Ste\,Fo})^{1/4}$. When the order of magnitude of the group $(\mathrm{Ste\,Fo})^{1/4}$ is greater than 1, the size of the melt fraction is ruled by the horizontal intrusion layer. When its order of magnitude is less than 1 (as in the numerical experiments of Reference 3 and Figure 6), the melt fraction is dominated by the boundary-layer convection that erodes the nearly vertical portion of the two-phase interface (i.e., by the area A_1). This result does not mean that the intrusion-layer effect is entirely negligible when the dimensionless time Ste Fo is less than 1:

Ste Fo	1	0.1	0.01	0.001
$0.725\ (\mathrm{Ste\,Fo})^{1/4}$	0.725	0.41	0.23	0.13

Thus the melt-fraction effect of the intrusion layer continues to be felt even when the time-group Ste Fo is as low as 10^{-3}.

Acknowledgment

This work was sponsored by the Electric Power Research Institute through contract no. RP 8006-4 under the management of Dr. Jong H. Kim.

References

1 Lacroix, M. Computation of heat transfer during melting of a pure substance from an isothermal wall. *Num. Heat Transfer Part B*, 1989, **15**, 191–210
2 Zhang, Z. and Bejan, A. Melting in an enclosure heated at constant rate. *Int. J. Heat Mass Transfer*, 1989, **32**, 1063–1076
3 Jany, P. and Bejan, A. Scales of melting in the presence of natural convection in a rectangular cavity filled with porous medium. *J. Heat Transfer*, 1988, **110**, 526–529
4 Kazmierczak, M., Poulikakos, D., and Pop, I. Melting from a flat plate embedded in porous medium in the presence of steady natural convection. *Num. Heat Transfer*, 1986, **10**, 571–581
5 Bejan, A. Theory of melting with natural convection in an enclosed porous medium. *J. Heat Transfer*, 1989, **111**, 407–415
6 Bejan, A. Analysis of melting by natural convection in an enclosure. *Int. J. Heat Fluid Flow*, 1989, **10**, 245–252
7 Cheng, P. Heat transfer in geothermal systems. *Adv. Heat Transfer*, 1979, **14**, 1–105
8 Weber, J. E. The boundary layer regime for convection in a vertical porous layer. *Int. J. Heat Mass Transfer*, 1975, **18**, 569–573